

See discussions, stats, and author profiles for this publication at: <https://www.researchgate.net/publication/328982367>

Electrodes Based on Zeolites Modified with Cobalt and/or Molybdenum for Pesticide Degradation. Part I: Physicochemical Characterization and Efficiency of the Electrodes for O₂ Redu...

Article · November 2018

DOI: 10.1007/s12678-018-0500-4

CITATIONS

0

READS

131

8 authors, including:



Ana María Méndez-Torres

University of Chile

3 PUBLICATIONS 1 CITATION

SEE PROFILE

Francisco Fernández

University of Santiago, Chile

4 PUBLICATIONS 12 CITATIONS

SEE PROFILE



Elizabeth G Garrido-ramirez

Universidad Andrés Bello

11 PUBLICATIONS 574 CITATIONS

SEE PROFILE



Nestor Escalona

Pontificia Universidad Católica de Chile

100 PUBLICATIONS 1,265 CITATIONS

SEE PROFILE

Some of the authors of this publication are also working on these related projects:



Advanced Materials Characterization [View project](#)



Novel magnetic materials based Nb and Si [View project](#)



Electrodes Based on Zeolites Modified with Cobalt and/or Molybdenum for Pesticide Degradation. Part I: Physicochemical Characterization and Efficiency of the Electrodes for O₂ Reduction and H₂O₂ Production

Ana María Méndez-Torres^{1,2} · Jorge Castro^{2,3} · Francisco Fernández² · Elizabeth Garrido-Ramírez^{4,5} · Néstor Escalona^{6,7} · Claudio Gutiérrez⁸ · José F. Marco⁸ · M. Soledad Ureta-Zañartu²

Published online: 16 November 2018

© Springer Science+Business Media, LLC, part of Springer Nature 2018

Abstract

With the purpose of obtaining inexpensive electrodes for the degradation of organic pesticides by the electro-Fenton reaction, the required H₂O₂ being obtained by the 2-electron reduction of dissolved O₂, we have prepared glassy carbon electrodes coated with a mixture of graphite with Mo- and/or Co-modified zeolites. Three zeolites were used, Linde type A (ZA), Faujasite (ZY), and MFI (ZSM5), whose maximum possible cation exchange, directly given by the Al/Si ratio, and their hydrophilicity increases in the order ZSM5 < ZY < ZA. The zeolites were modified with Mo and/or Co by the wet impregnation method and characterized by different techniques. The outer surfaces of the three Mo-modified zeolites showed Mo-containing grains (in ZA) or needles (in ZY and ZSM5), which could be largely washed away with hot water. Electrodes were made by depositing on a disc of glassy carbon (GC) a mixture of graphite, zeolite, and a binder. Quite unexpectedly, the cyclic voltammograms (CVs) of the three Mo-modified zeolites showed at least five pairs of anodic–cathodic peaks, which we assume are due to the presence of the Mo₇O₂₄^{6−} isopolyoxomolybdate anion, proceeding from the impregnating solution, and anchored on the zeolites' surface. With a rotating ring-disc electrode, the highest efficiency for H₂O₂ production at −0.2 V_{RHE}, namely, 12.7%, was obtained with the GC/graphite-(CoMo-exchanged ZA) electrode, but this efficiency decreased with time. On the contrary, the three zeolites modified only with Mo were stable in 4-h electrolyses at −0.2 V_{RHE} and yielded the highest H₂O₂ concentrations, which we attribute to the Mo₇O₂₄^{6−} isopolyoxomolybdate anchored on the zeolites. The H₂O₂ yield was the same for the three Mo-modified zeolites, irrespective of their exchange capacity and hydrophobic/hydrophilic character.

Keywords Oxygen reduction · Hydrogen peroxide · Mo- and/or Co-modified zeolites · Graphite-modified zeolite electrodes · Electrolysis

Electronic supplementary material The online version of this article (<https://doi.org/10.1007/s12678-018-0500-4>) contains supplementary material, which is available to authorized users.

✉ M. Soledad Ureta-Zañartu
soledad.ureta@usach.cl

¹ Present address: Facultad de Ciencias Químicas y Farmacéuticas, Universidad de Chile, Santiago, Chile

² Departamento de Ciencias del Ambiente, Facultad de Química y Biología, Universidad de Santiago de Chile, Av. L. B. O'Higgins 3363, Casilla 40, Correo 33, Santiago, Chile

³ Present address: Facultad de Ciencias, Universidad de Chile, Santiago, Chile

⁴ Departamento de Ecología y Biodiversidad, Universidad Andres Bello, República 440, Santiago, Chile

⁵ Centro de Investigación para la Sustentabilidad, Facultad de Ciencias de la Vida, Universidad Andres Bello, República 440, Santiago, Chile

⁶ Departamento de Ingeniería Química y Bioprocesos, Escuela de Ingeniería, Pontificia Universidad Católica de Chile, Avenida Vicuña Mackenna 4860, Macul, Santiago, Chile

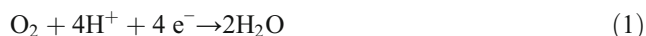
⁷ Departamento de Química Física, Facultad de Químicas, Pontificia Universidad Católica de Chile, Santiago, Chile

⁸ Instituto de Química Física “Rocasolano”, CSIC, C. Serrano, 119, 28006 Madrid, Spain

Introduction

In this work we have studied the 2-electron reduction of molecular oxygen to H_2O_2 , of interest in the so-called advanced oxidation process (AOP) [1] of which electro-Fenton processes are the best known [2–4]. These processes, based on the in situ production of hydrogen peroxide, which upon further reaction generates hydroxyl radicals [1], could be of interest for the degradation of organic pesticides.

In acidic media, the oxygen reduction reaction (ORR) is given by Eqs. (1) or (2),

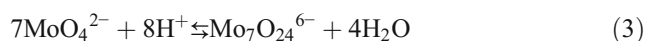


yielding water (1) or hydrogen peroxide (2), respectively.

Inexpensive zeolite-based electrodes have interesting properties, since zeolites are aluminosilicates with many channel networks, which provide ideal cavities for chemical reactions [5]. Both the hydrophilicity and the exchange capacity increase with increasing Al/Si atomic ratio [6], an excellent review being given in refs. [7, 8]. Commercial zeolites are usually neutralized with alkaline and alkaline-earth metals, which can be easily exchanged with cations of transition metals [9–11]. Moreover, zeolites can be used as support for more than one metal, then simulating bimetallic alloys. So, El-Shafei et al. [12] incorporated Pd and Au into graphite/zeolites electrodes and the sequence of immersion as well as the concentration of metal ions determining the alloy composition. The acidity and pore diameter of the zeolites must also be considered for each particular application [13]. Electrodes based on ZA doped with Ag have been proposed as hydrogen peroxide [14] and oxygen [15] sensors.

Different oxides have been used as catalysts in electrode preparation [16, 17]. Oxides of molybdenum, either alone or accompanied by cobalt, have been widely studied in heterogeneous catalysis and recently in electrocatalysis [18]. The active species, usually formed by calcination, depends on the support structure and composition [19]. The extended tunnels between the MoO_6 octahedra serve as channels and intercalation sites for mobile ions such as H^+ and Li^+ [20], making MoO_6 a good redox promoter. Saji and Lee [20] published an excellent review of the electrochemistry of Mo and its oxides.

In acidic aqueous media, the molybdate anion is in equilibrium with heptamolybdate, an isopolyoxomolybdate anion (the prefix *iso* indicates the absence of nonmetallic atoms like P or Si):



In this work, we have prepared inexpensive electrodes based on zeolites modified with molybdenum and/or cobalt which could be used for the degradation of pesticides by the

electro-Fenton reaction with the hydrogen peroxide generated by the reduction of dissolved oxygen. Three zeolites with very different Si/Al molar ratios were characterized by nitrogen adsorption–desorption isotherms, scanning electron microscopy (SEM) coupled with energy-dispersive X-ray spectroscopy (EDS), X-ray diffraction (XRD), X-ray photoelectron spectroscopy (XPS), and Fourier-transform infrared spectroscopy with attenuated total reflection (FTIR–ATR). A homogenized graphite–zeolite–binder mixture was deposited on GC discs, and the activity of these GC/graphite–zeolite electrodes for the global oxygen reduction and their efficiency for H_2O_2 production was determined. The activity of these electrodes for the degradation of 2,4,6-trichlorophenol will be given in part II.

Experimental

Characterization of the Zeolites

As in our previous work [21], three commercial zeolites of different hydrophilicity were used, since this property affects their activity for oxygen reduction [22]: Linde type A (ZA), a low-silica zeolite with Si/Al = 1 (Analytical North Harrison Road, Bellefonte, USA); Faujasite (ZY), an intermediate-silica zeolite with Si/Al = 2.5 (Aldrich, St. Louis, USA); and MFI (ZSM5), a high-silica zeolite with Si/Al = 50 (Zeolyst International, KS, USA). The (monovalent cation)/Si exchange capacities of these zeolites, directly given by the Al/Si ratio, were 1, 0.4, and only 0.02, respectively, decreasing in the same order as their hydrophilicity. The zeolites were modified with molybdenum and/or cobalt by the wet impregnation method [19, 23, 24] using $(\text{NH}_4)_6\text{Mo}_7\text{O}_{24} \cdot 4\text{H}_2\text{O}$ (Merck, > 99%) and $\text{Co}(\text{NO}_3)_2 \cdot 6\text{H}_2\text{O}$ (Sigma-Aldrich, > 98%), respectively, as precursors. (In the case of Mo, its cationic species, which obviously are the only ones that can be exchanged with the zeolite cations, can be present only in very acidic media [25, 26]. Therefore, at pH 3, the heptamolybdate anion could enter into zeolite only as a neutral salt, not by exchange). Briefly, 2.5 g zeolite was modified with 3 wt% metal $(\text{NH}_4)_6\text{Mo}_7\text{O}_{24} \cdot 4\text{H}_2\text{O}$ and/or $\text{Co}(\text{NO}_3)_2 \cdot 6\text{H}_2\text{O}$ and 60 mL of distilled water, using the wet impregnation method [19, 23, 24]. The initial pH was 5.3 for the heptamolybdate solution and 6.2 for the cobalt nitrate solution. The zeolites modified with both cations, Mo and Co, were prepared with solutions containing both metals. The modified zeolites are identified as Z_M , where Z can be ZA, ZY, or ZSM5 and M: Mo, Co, or both.

The morphology of the zeolites was characterized by scanning electron microscopy (SEM) with a PhenomProX equipment, PhenomWorld or a Bruker Vega 3 Tescan. Both instruments were coupled to an energy-dispersive X-ray spectroscopy (EDS) instrument with an electron accelerating voltage

of 15 kV. The powdered samples were fixed on a double-sided adhesive carbon tape.

X-ray powder diffraction was carried out with a Bruker D8 Advance diffractometer with Bragg–Brentano geometry and FTIR–ATR spectroscopy with a Bruker-Platinum-ATR instrument. The BET surface areas (S_{BET}) and the mesopore, micropore, and total pore volumes were determined by nitrogen adsorption–desorption isotherms at 77 K using a 3-FLEX instruments. A PHOIBOS-150 SPECS analyzer under a base pressure of 3×10^{-10} Torr was used for the XPS determination of the oxidation state of the metal cations, with Al $K\alpha$ radiation for the Co 2p spectra and Mg $K\alpha$ radiation for the Mo 3d and O 1s spectra. Wide-scan and narrow-scan spectra were recorded with a constant pass energy of 100 and 20 eV, respectively. Binding energies were referenced to the C 1s binding energy of the adventitious carbon layer, taken to be 284.6 eV. The quantitative XPS analysis was carried out with the Multiquant XPS software [27].

Electrode Preparation

Graphite (99.98% Riedel de Haën), with a particle size between 2.12 and 6.10 μm , was previously cleaned by heating under nitrogen at 120 $^{\circ}\text{C}$ for 4 h, cooled, and stored under nitrogen in a desiccator. The glassy carbon/graphite-modified zeolite electrodes (GC/g- Z_{M} , where M represents the transition metal cation) were prepared as previously reported [21]. Briefly, 30 μL of a suspension of 19 mg of modified zeolite, 50 mg graphite, and 0.5 mL Nafion® perfluorinated ion-exchange resin in 4 mL distilled water was homogenized in an ultrasonic bath for 2 h, then the homogenized suspension was deposited on the surface of a glassy carbon electrode of 0.071 or 0.13 cm^2 geometric area (CH Instruments and ALS (BAS), respectively), and finally the water was evaporated in an oven at 60 $^{\circ}\text{C}$ for 30 min. The zeolite loading, referred to the geometric area, was 3.3 mg cm^{-2} , with the exception of the ring-disc electrodes, in which the coating was smaller, 1.83 mg cm^{-2} , in order to avoid its detachment at high rotation rates, and of the electrodes in long-time electrolysis, in which a loading of 2.0 mg cm^{-2} was used. Blank electrodes contained the same amount of the unmodified zeolites. The current densities (j) are referred to the geometric electrode area. The roughness factor, $R_{\text{F(GC)}}$, of the GC/g- Z_{M} electrodes relative to that of GC, as determined from the double layer capacitance [21], was about 150 ± 20 for the 3.3- mg cm^{-2} zeolite loading. All the experiments were carried out in a 0.1- mol L^{-1} Na_2SO_4 solution adjusted to pH 3 with 0.5 M H_2SO_4 . The electrodes were stabilized by repetitive potential cycling at 0.02 V s^{-1} .

Electrochemical Measurements

A one-compartment three-electrode cell with a large area Pt helix as auxiliary electrode, an Ag/AgCl/3 M KCl reference electrode immersed in a Luggin capillary closed with a Pt

wire, and an electrochemical workstation CHI 660C (CHInstruments) with an RRDE-RA Ring-Disk rotator or an Autolab PGstat 128 N, were used. The potentials in the text have been referred to the reversible hydrogen electrode (RHE) by adding

$$E_{\text{Ag/AgCl, 3 MKCl}} \text{ vs SHE} + 0.0591\text{pH} = 0.209 + 0.177 = 0.386 \text{ V} \quad (4)$$

to the potentials measured vs the Ag/AgCl electrode. Long-time electrolyses at -0.2 V of O_2 -saturated solutions were performed in a one-compartment cell, using a GC disc of 0.50 cm^2 geometric area (Carbon Lorraine, France).

Determination of Hydrogen Peroxide

Samples of the electrolyte solution were taken during the 4-h electrolyses, and their H_2O_2 concentration was determined by UV–vis spectroscopy at 400 nm using the potassium titanium (IV) oxalate method [28, 29].

Results and Discussion

Characterization of the Modified Zeolites

Nitrogen Adsorption/Desorption Isotherms

The nitrogen isotherms of the unmodified zeolites have been reported in a previous work [21], and now we have obtained those of the Mo, Co, and Co–Mo zeolites (Fig. S1, in the Supplementary Materials). Both unmodified and modified ZA and ZSM5 showed hysteresis at high relative pressures, which remained after modification, and the adsorption curve displayed an abrupt increase in the high-pressure region, especially in ZA, evidencing the presence of micro- and mesopores, as shown in Table 1.

Modification of ZA with Co produced only a small decrease (13%) of its surface area (curve 2 in Fig. S1a). On the contrary, the modification with Mo (curve 3 in Fig. S1a) or Co–Mo (curve 4 in the same figure) brought about a huge decrease of about 95% of the surface area, showing that Mo compounds clog the surface of ZA, perhaps because of its highly hydrophilic character. Correspondingly, Mo reduced the micropore volume of ZA by 94% and the mesopore volume by 80%.

ZY (Fig. S1b), which is the zeolite with the highest surface area, yielded nearly flat type I isotherms, characteristic of microporous materials, with the isotherms showing no hysteresis. The modification with Co reduced the surface area by only 4%, with Mo (curve 3) by 26%, and with both Co and Mo (curve 4) by 36%.

Table 1 BET surface area and porosity of the unmodified and modified zeolites

Zeolite	S_{BET} $\text{m}^2 \text{g}^{-1}$	Pore volume $\text{cm}^3 \text{g}^{-1}$	Micropore volume $\text{cm}^3 \text{g}^{-1}$	Mesopore volume $\text{cm}^3 \text{g}^{-1}$
ZA	415	0.28	0.18	0.10
ZA-Co	361	0.23	0.16	0.07
ZA-Mo	15	0.03	0.01	0.02
ZA-CoMo	23	0.06	0.01	0.05
ZY	764	0.34	0.34	0.00
ZY-Co	733	0.32	0.32	0.00
ZY-Mo	563	0.24	0.24	0.00
ZY-CoMo	490	0.26	0.26	0.00
ZSM5	364	0.22	0.16	0.06
ZSM5-Co	n.d.	n.d.	n.d.	n.d.
ZSM5-Mo	266	0.14	0.12	0.02
ZSM5-CoMo	287	0.18	0.15	0.03

The surface area of ZSM5 (curve 1 in Fig. S1c) was slightly lower than that of ZA. The modification with Mo (curve 3) reduced the surface area of ZSM5 by 27%. In the case of ZSM5_{CoMo}, the decrease was lower, 21%, because Co decreased the concentration of Mo (Table 3).

SEM-EDS

SEM micrographs of the different zeolites are shown in Fig. 1. The images in the first column correspond to the unmodified ZA, ZY, and ZSM5 zeolites. ZA shows cubic particles 2.9–3.5 μm in diagonal and zones where these particles are agglomerated. ZY has a nonuniform structure with many aggregates, the smallest particles showing a cubic structure with a diagonal of 1.4–1.6 μm . And ZSM5 consisted of dust-like particles of about 0.8 μm .

EDS analyzes a layer 1–2 μm deep, and its detection limit is about 0.5 at.%. The atomic compositions of the ZA, ZY, and ZSM5 zeolites, estimated by EDS, are given in Table 2. The Si/Al ratios were 1.0 for ZA and 2.4 for ZY, in excellent agreement with the nominal ratios of 1.0 and 2.5, respectively. On the contrary, the Si/Al ratio of ZSM5 was 23.3, about half the nominal ratio of 50. The total positive charge of exchanged cations in ZA was 7.8, in fair agreement with the Al content (11%). And the total positive charge of exchanged cations in ZY was 6, in fair agreement with the Al content (7.8%). No cations were detected in ZSM5, because its maximum possible (exchanged monovalent cation)/Si ratio, 0.02, is negligible, within the error margin of EDS.

The SEM images of the Co-modified ZA, ZY, and ZSM5 zeolites (second column in Fig. 1) do not show major changes as compared with the unmodified zeolites. The Co concentration was near the detection limit at the best and decreased with increasing Si/Al ratio, as expected: it was 1.7% for ZA_{Co},

0.14% for ZY, and 0% for ZSM5_{Co} (Table 3). Consequently, their standard deviations were as high as $\pm 71\%$.

The micrographs of the Mo-modified ZA, ZY, and ZSM5 zeolites (third column in Fig. 1) showed important changes with respect to both unmodified and Co-modified zeolites. ZA_{Mo} shows, besides the original cubic particles, large grains. As for ZY_{Mo} and ZSM5_{Mo}, they showed new, Mo-containing needles on the outer surface, longer and much more abundant in ZY_{Mo} than in ZSM5_{Mo}. These latter needles could be washed away with hot water [30], as can be seen in the images in the fourth column in Fig. 1. However, in ZA_{Mo-w}, some grains remained after washing. In agreement with this, Mo mapping of washed ZA_{Mo-w} showed some Mo well dispersed on the zeolite (image ZA_{Mo} (2) in Fig. S2). The Mo mapping coincided with that of Ca, perhaps indicating the formation of a Ca molybdate (image ZA_{Mo} (2) in Fig. S2). As in the case of Co, the concentrations of Mo were mostly nearly the detection limit of EDS, and consequently, their standard deviations were as high as $\pm 86\%$ (Table 3).

When the zeolites were modified with both Co and Mo (fifth column in Fig. 1), again grains appeared in ZA_{CoMo} and needles in both ZY_{CoMo} and ZSM5_{CoMo}, although to a lesser extent than in the zeolites modified only with Mo. The concentrations of Co and Mo in the original particles of the three zeolites were 0 or nearly so (Table 3). There was some Co in the grains of ZA_{CoMo}, but a negligible amount in the needles of ZY_{CoMo}, and none at all in the needles of ZSM5_{CoMo} (Table 3). There was Mo in the grains of ZA_{CoMo} and in the needles of ZY_{CoMo}, but barely so in the needles of ZSM5_{CoMo} (Table 3). However, even in the grains and needles, the Co and Mo concentrations were near the detection limit of EDS, and therefore, their standard deviations were as high as ± 40 and $\pm 86\%$, respectively.

No K was observed in the unmodified zeolites. Therefore, the K in the modified zeolites came from the cold washing

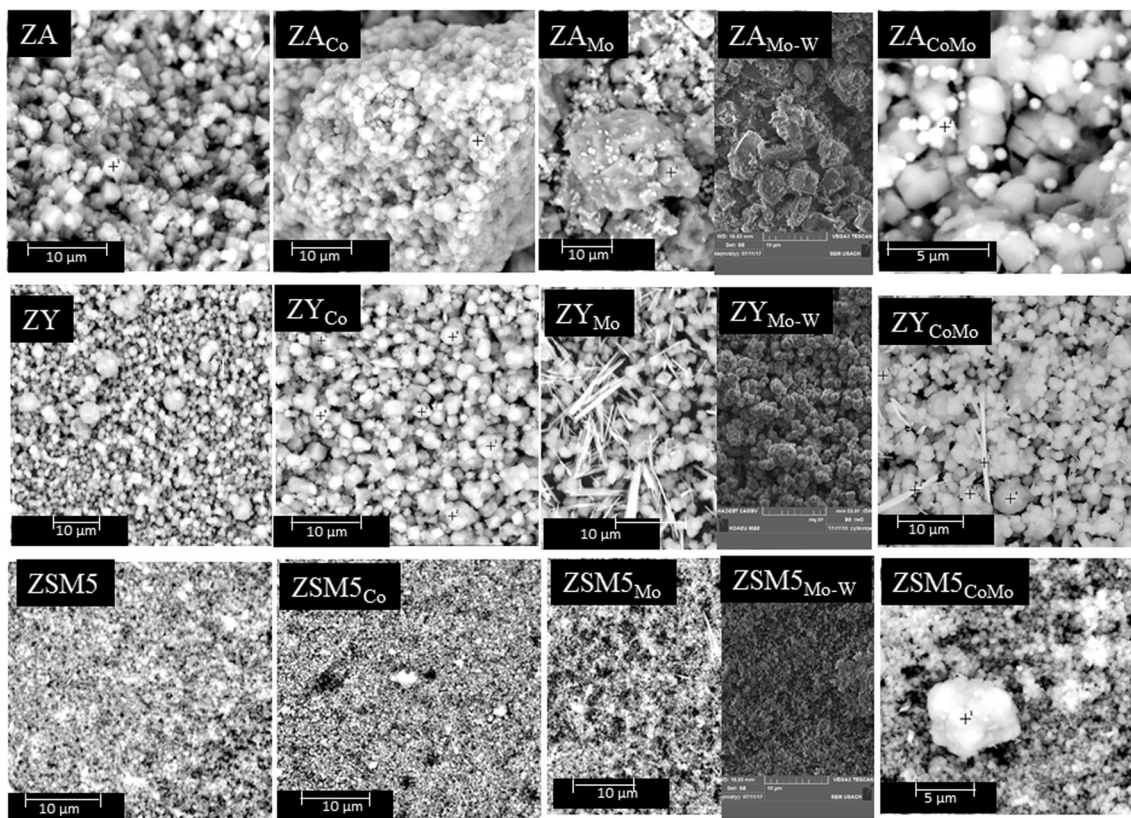


Fig. 1 SEM images of unmodified zeolites (first column) and of zeolites modified with cobalt (second column), molybdenum (before and after washing with hot water (w)) (third column), and both cobalt and molybdenum (fourth column)

solution and did not disappear after washing with hot water, as observed by Tran et al. [31] with ZY.

XRD

The XRD patterns of all the unmodified and modified zeolites shown in Fig. 2 correspond to the ZA, ZY, and ZSM5 zeolites. Curves 1 are the patterns of the unmodified zeolites, curves 2 those of the Co-modified zeolites, curves 3 those of the Mo-modified zeolites, and curves 4 those of the both Co- and Mo-modified zeolites. In general, all the diffraction peaks of the original zeolites (marked as *) [32] were retained in the

modified ones, which, together with the SEM results, suggest that only a very small fraction of Co and/or Mo was dispersed inside the zeolite framework, the larger fraction of Co and Mo forming grains and/or needles on the outer surface of the zeolites.

The pattern of ZA_{Co} (curve 2 in Fig. 2—ZA) shows small additional peaks at $2\theta = 26.3^\circ$, 35.9° , and 41.7° (dashed lines), which could be due to Co_3O_4 [33] or CoO species [34], this last assignment agreeing with the XPS results (see below).

The pattern of ZA_{Mo} (curve 3 in Fig. 2—ZA) shows a very intense new diffraction peak at 26.3° and three small peaks at 18.6° , 47.3° , and 49.5° (dotted lines in Fig. 2). These four peaks were also observed, but much broader (less crystallinity), in the pattern of ZA_{CoMo} (curve 4 in Fig. 2—ZA), which also showed the peaks of Co oxide(s). Since MoO_3 can form different structures or combinations of them, it is difficult to assign the peaks.

Interestingly, the patterns of the ZY_{Mo} and ZY_{CoMo} (curves 3 and 4, respectively, in Fig. 2—ZY) do not show at all the very intense diffraction peak at 26.3° , but they do show the same small peaks at 18.6° (here at 16.6°) and 47.1° (here at 47.3°) of the Mo compound in ZA_{Mo} . Two small peaks at 12.5° and 16.6° can be assigned to hexagonal MoO_3 [35–37], in agreement with the needles observed by SEM. These peaks are very small because the needles are only on

Table 2 Particle size (SEM) and atomic composition (%) (EDS) of the unmodified zeolites

Zeolite	Particle size/ μm	Atomic percentage			Cations
		O	Si	Al	
ZA	2.9–3.5	73 ± 2	11 ± 1	11 ± 1	Ca 2.3 ± 0.6 Na 1.8 ± 0.7 Mg 0.7 ± 0.2
ZY	1.4–1.6	67 ± 3	19 ± 2	7.8 ± 0.6	Na 6.0 ± 0.7
ZSM5	0.8	71 ± 5	28 ± 5	1.2 ± 0.3	0

Table 3 Atomic composition (%) (EDS) of the modified zeolites

Zeolite	Shape of Mo surface deposits	Atomic percentage					
		Co	Mo	Ca	Na	Mg	K
ZA-Co		1.7 ± 0.9		3.5 ± 0.8	0.3 ± 0.2	0.9 ± 0.2	3.7 ± 0.8
ZY-Co		0.14 ± 0.10		0	1.4 ± 0.4	0	3.3 ± 1.1
ZSM5-Co		0		0	0	0	0.6 ± 0.2
ZA-Mo	Cubic grains		2.3 ± 1.8	2.2 ± 1.2	0.7 ± 0.5	1.2 ± 0.4	6.4 ± 3.8
			10 ± 5	7.4 ± 3.4	0.5 ± 0.1	0.9 ± 0.3	2.1 ± 1.0
ZA-Mo, washed			4.0 ± 0.6	3.9 ± 0.2	0.4 ± 0.1	1.1 ± 0.1	4.0 ± 0.2
ZY-Mo	Cubic needles		0.9 ± 0.4	0	1.4 ± 0.4	0	4.2 ± 1.5
			7 ± 6	0	1.1 ± 0.2	0	6.7 ± 1.3
ZY-Mo, washed			0.7 ± 0.3	0	2.4 ± 0.2	0	4.5 ± 0.2
ZSM5-Mo	Powder needles		0.2 ± 0.1	0	0	0	1.2 ± 0.8
			1.4 ± 1.1	0	0	0	0.7 ± 0.3
ZSM5-Mo, washed			0.05 ± 0.02	0	0	0	1.1 ± 0.1
ZA-CoMo	Cubic grains	0	0.5 ± 0.4	0.8 ± 0.2	0	0.4 ± 0.1	4.2 ± 2.4
			1.4 ± 0.4	5.4 ± 2.0	3.2 ± 3.2	0.4 ± 0.2	0.9 ± 0.2
ZY-CoMo	Cubic needles	0.05 ± 0.02	0	0	0.6 ± 0.3	0	2.9 ± 2.0
			0.11 ± 0.04	7 ± 6	0	1.0 ± 0.5	0
ZSM5-CoMo	Powder needles	0	0	0	0	0	0.3 ± 0.1
			0	0.3 ± 0.1	0	0	0

the outer surface of ZY, while XRD is a bulk technique. Some Mo could have entered the pores of the zeolite as a neutral species, in agreement with the Mo mapping of washed ZA_{Mo} (image ZA_{Mo} (2) in Fig. S2), which shows that Mo is well

dispersed in the zeolite, although most of the Mo-containing grains on the outer surface had been washed away. This is supported by the work of Tran et al. [31], who prepared a molybdenum oxide catalyst using Mo heteropoly acids for

Fig. 2 XRD patterns of unmodified zeolites (curves 1) and of zeolites modified with cobalt (curves 2), molybdenum (curves 3), and both cobalt and molybdenum (curves 4). Peaks are marked as follows: (*): unmodified zeolites; (red dashed lines): cobalt oxides; and (green dotted lines): molybdenum compounds

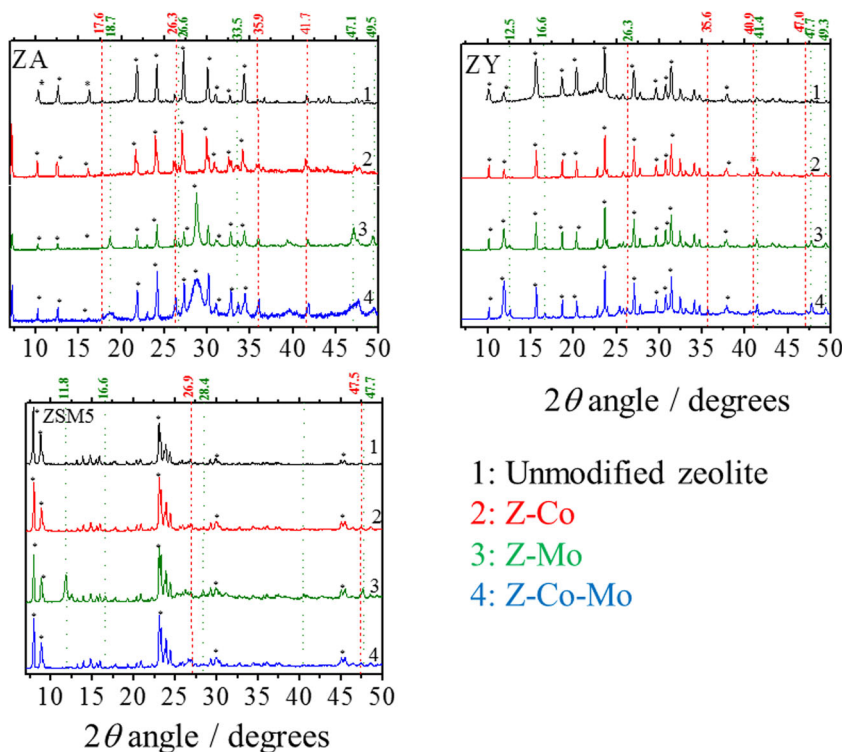


Table 5 Electrochemically active molybdenum loading, half-sum potential, and peak separation of the redox couples. Data taken from Fig. 6

Electrode: GC/graphite-	[Mo]# 10 ⁻⁸ mol cm ⁻²	$E_{1/2}$ /V vs RHE						ΔE_p /V					
		c1/a1	c2/a2	c3/a3	c4/a4	c5/a5	c6/a6	a1-c1	a2-c2	a3-c3	a4-c4	a5-c5	a6-c6
-ZA _{Mo}	8.5	0.09	0.18	0.34	0.56	0.69	–	0.08	0.07	0.08	0.04	0.06	–
-ZA _{Mo} *	7.6	–0.09	–	–	–	0.78	–	0.24	–	–	–	0.08	–
-ZY _{Mo}	11.0	–0.01	0.11	–	0.56	0.68	0.81	0.08	0.23	–	0.05	0.07	0.07
-ZY _{Mo} *	6.2	–0.09	0.09	–	0.57	0.68	0.79	0.02	0.13	–	0.06	0.03	0.02
-ZSM5 _{Mo}	24.2	–0.10	0.09	0.29	0.48	0.64	–	0.07	0.24	0.18	0.17	0.12	–
-ZSM5 _{Mo} *	6.2	–0.05	0.09	0.21	0.42	0.69	–	0.10	0.10	0.08	0.03	0.15	–

[Mo]#: electrochemically active Mo concentration from the positive scan in CVs at 0.02 V s⁻¹

$E_{1/2} = 1/2(E_{p_{an}} + E_{p_{cat}})$; $\Delta E_p = E_{p_{an}} - E_{p_{cat}}$

*Washed with hot water

encaging molybdenum oxide in ZY. These authors observed no difference in the XRD patterns, which they attributed to a high dispersion of Mo.

The patterns of both ZSM5_{Co} and of ZSM5_{CoMo} (curves 2 and 4, respectively, in Fig. 2—ZSM5) showed no Co peaks, in agreement with the 0% Co concentration in these two zeolites (Tables 3 and 5, respectively). In a similar way, the patterns of both ZSM5_{Mo} and ZSM5_{CoMo} (curves 3 and 4, respectively, in Fig. 2—ZSM5) showed almost no Mo peaks, in agreement with their very low Mo concentrations (Tables 4 and 5, respectively). This is in agreement with the micrographs of ZSM5_{Co} and ZSM5_{CoMo} (Fig. 1), which show no grains and nearly no needles, respectively.

The XRD patterns of the samples washed with hot water and/or calcined (Fig. S3) evidence that some Mo was not washed away, in agreement with the small, but finite, Mo concentration (Table 3) and with the Mo mapping (image

ZY_{Mo} (2) in Fig. S2), which shows a significant presence of Mo.

XPS

XPS analyzes only the uppermost (3–10 nm) layer of the samples, and its detection limit is 0.1–1 at.%. The XPS wide-scan spectra of the original zeolites (not shown) agree qualitatively with those expected from the nominal

Table 4 Atomic ratios of the unmodified and modified zeolites as determined by XPS

Zeolite	Co/Si	Mo/Si	O/Si	Si/Al
ZA	–	–	4.6	3.7
ZA-Co	0.86	–	5.7	4.0
ZA-Mo	–	0.58	5.7	2.6
ZA-CoMo	0.13	0.67	7.6	4.2
ZY	–	–	3.7	3.9
ZY-Co	0.11	–	4.5	3.5
ZY-Mo	–	0.30	5.1	3.6
ZY-Mo, washed	–	≈ 0.01	–	–
ZY-CoMo	0.02	0.61	6.2	3.6
ZSM5	–	–	3.9	–
ZSM5-Co	0.01	–	3.1	–
ZSM5-Mo	–	0.39	5.0	–
ZSM5-CoMo	0.01	0.06	3.2	–

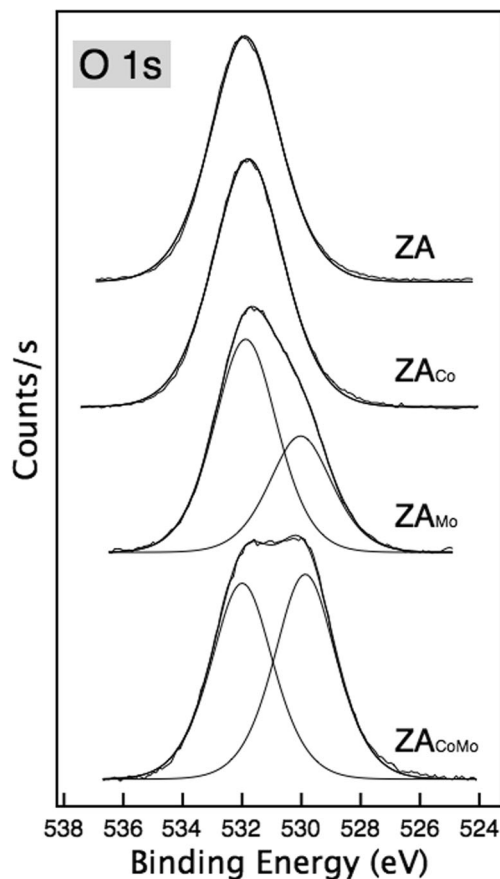
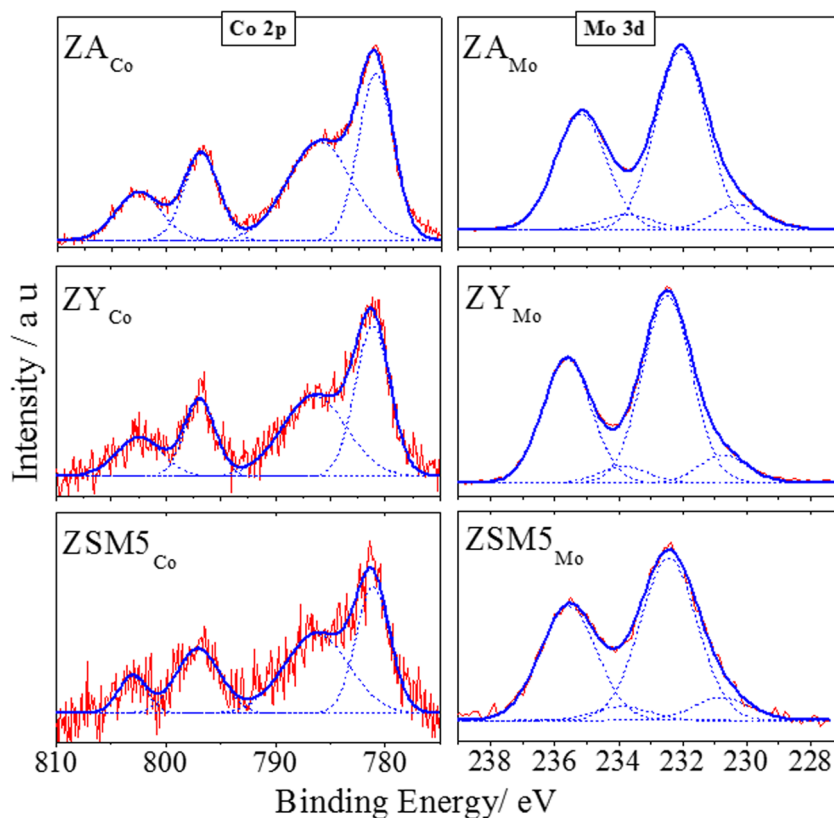
**Fig. 3** XPS spectra of O1s in ZA, ZA_{Co}, ZA_{Mo}, and ZA_{CoMo}

Fig. 4 XPS spectra of Co 2p in Z_{Co} and XPS spectra of Mo 3d in Z_{Mo} . Thin lines: experimental data; thick and dashed lines: fitted curves



composition, the atomic ratios being given in Table 4. The Co/Si and Mo/Si ratios were very high: The Mo/Si ratio was 0.6 in ZA_{Mo} , 0.3 in ZY_{Mo} , and 0.4 in $ZSM5_{Mo}$. In stark contrast with this, the concentrations of Co and Mo obtained by EDS (Table 3) were very low, a few atomic percent at the most. This clearly shows that Co and Mo were mostly on the outer surface. Interestingly, the XPS data show that the Co-modified ZSM5 sample contains a small Co concentration that was undetected by EDS, clearly showing again that Co was mostly on the surface.

The narrow-scan O 1s spectra of the various ZA samples are given in Fig. 3. The O 1s spectrum of the unmodified ZA shows a relatively narrow single peak with a binding energy of 531.8 eV. The O 1s spectrum of ZA_{Co} was very similar to that of ZA, but that of ZA_{Mo} showed an additional oxygen contribution at 530.0 eV which accounted for 35% of the spectral area. This binding energy can be associated mainly with the presence of OH groups, although a contribution to that peak of an overlapping Si–O signal cannot be discarded [38]. The O 1s spectrum of ZA_{Co} was very similar to that of ZA, but that of ZA_{Mo} showed an additional oxygen contribution at 530.0 eV which accounted for 35% of the spectral area. This binding energy is characteristic of metal–oxygen bonds [38] and is due to the high Mo/Si ratio, 0.58 (Table 4). The contribution at 530.0 eV increased to 51% in ZA_{CoMo} , also due to its high Mo/Si ratio, 0.67 (Table 4). A similar increase of the oxygen contribution at 530.0 eV was observed in ZY and ZSM5 upon

modification with Mo, due to their high Mo/Si ratios, 0.30 and 0.39, respectively, but not for $ZSM5_{CoMo}$, since its Mo/Si ratio was only 0.06 (Table 4).

The Co 2p and Mo 3d narrow-scan spectra are shown in Fig. 4. The Co 2p spectra of ZA_{Co} , ZY_{Co} , and $ZSM5_{Co}$ are virtually identical and show several contributions. The Co 2p spectrum is composed of a spin-orbit doublet with binding energies of 781.3 and 797.1 eV for the Co 2p_{3/2} and Co 2p_{1/2} core levels, respectively. The spectra also show strong shake-up structure at 786.9 and 802.8 eV, this satellite structure being characteristic of Co²⁺. The binding energies of the corresponding core levels are slightly higher than those expected for a typical Co²⁺ species such as those encountered in CoO or Co²⁺-containing spinels, for example [39], and are more like those shown by Co in ion-exchange sites in zeolites [40, 41].

The Mo 3d spectra of the three Mo-modified zeolites are also shown in Fig. 4. Again, the three spectra are very similar, with a main doublet at 232.0 and 235.1 eV, characteristic of Mo(VI), whereas the very weak peaks at 230.2 and 233.3 eV have been associated with Mo(IV) [42]. Most probably the latter peaks were produced by photoreduction of Mo(VI) during the very long times required for obtaining spectra of the very low amounts of Mo in the samples [43]. The Mo/Si ratio in the washed and washed and calcined ZY_{Mo} was very low, around 0.01 (Table 4), which indicates that most of the Mo had been removed from the zeolite.

The XPS instrument used did not have the lateral resolution required for analyzing only the grains and needles (not the zeolite bulk) that appeared on the surface of Mo- and both Co- and Mo-modified zeolites.

ATR-FTIR Spectroscopy

The FTIR spectra of the ZA, ZY, and ZSM5 zeolites are shown in Fig. 5, in which curves 1 correspond to the unmodified zeolites, curves 2 to Co-modified zeolites, curves 3 to Mo-modified zeolites, curves 4 to Mo-modified zeolites after washing with hot water, and curves 5 to both Co- and Mo-modified zeolites. The fingerprint region of the spectra of ZA, ZY, and ZSM5 is given in Figs. S4a, S4b, and S4c, respectively, the labeling of the curves being the same as in Fig. 5.

The spectra of unmodified ZA, ZY, and ZSM5 (curves 1 in Fig. 5) have been widely reported [44–46] and show practically the same profile between 4000 and 1500 cm^{-1} . The 4000–3500- cm^{-1} spectral region, where the interaction between zeolites and adsorbed water molecules is observed (OH stretching mode of Si(OH)Al groups, Brønsted sites, silanol groups) [47], and that in the 2000–1300- cm^{-1} region, of the HOH bending of water [44], are noisy in the three zeolites, probably due to the presence of occluded water. The band at 2344 cm^{-1} has been attributed to a Lewis center without participation of Al^{3+} [47]. The spectrum of ZY shows an additional band at 3400 cm^{-1} (curve 1 in Fig. 5—ZY),

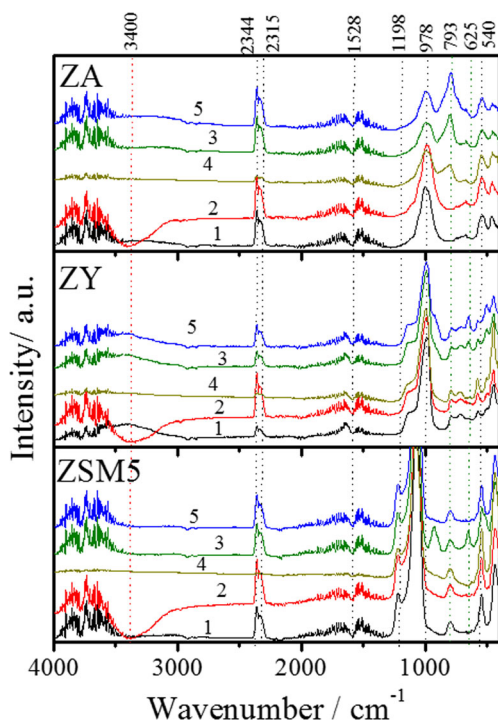


Fig. 5 FTIR–ATR spectra of zeolites. Curves 1: unmodified zeolites; curves 2: Co-modified zeolites; curves 3: Mo-modified zeolites; curves 4: Mo-modified zeolites after washing with hot water; and curves 5: both Co- and Mo-modified zeolites

reported for NaY only [48], which could be due to hydroxyl groups attached to extra framework alumina species. This region of the spectra changed drastically when the zeolites were exchanged with Co (curves 2 in Fig. 5), showing a virtually identical negative band at 3400 cm^{-1} in the three zeolites, which might correspond to a stretching Co–OH vibration [47]. This band was not observed in the CoMo–zeolites (curves 5 in Fig. 5), which implies that Mo affected the Co–Z structure.

In the fingerprint region (Fig. S4), the unmodified zeolites (curves 1) show a wide main peak, corresponding to the asymmetric and symmetric stretching modes of internal tetrahedra between 1198 and 850 cm^{-1} , depending on the zeolite. Thus, the band associated with the Si–O–T (T = Al or Si) internal asymmetric stretching vibration [49] was observed at 995 cm^{-1} in ZA, at 982 cm^{-1} in ZY, and at near 1067 cm^{-1} in ZSM5.

At lower wavenumbers, the Co-exchanged zeolites (curves 2 in Fig. S4) showed only small changes with respect to the unexchanged ones, indicating a small concentration of Co, in agreement with the SEM-EDS and XPS results. The bands of Co–O between 700 and 500 cm^{-1} could not be observed because the zeolites have many peaks in this region.

In the Mo-modified zeolites (curves 3 in Fig. S4), new bands appear at 792 cm^{-1} in ZA_{Mo} and at 648 cm^{-1} in ZY_{Mo} and ZSM5_{Mo} , which should be due to the large grains in ZA_{Mo} and to the needles in ZY_{Mo} and ZSM5_{Mo} , as observed by SEM. These bands could be due to a Keggin isopolyoxometalate structure [50]. The Si–O–Si bands near 990–1056 cm^{-1} decrease in ZA_{Mo} and ZSM5_{Mo} , which can be attributed to a change in the environment of the Si–O bond due to the incorporation of Mo. A new band near 800 cm^{-1} in the spectra of ZA_{Mo} , washed ZA_{Mo} , and ZA_{CoMo} (curves 3, 4, and 5, respectively, in Fig. 5) has been attributed to O–Mo–O stretching vibrations [31] and supports the presence of molybdenum oxide, as suggested by the EDS and XPS results. When the Z_{Mo} samples were washed with hot water, the band at 792 cm^{-1} in ZA_{Mo} and at 648 cm^{-1} in ZY_{Mo} and ZSM5_{Mo} (curves 4 in Fig. S4) disappeared, confirming the dissolution of the Mo-containing compounds (large grains in ZA_{Mo} and needles in ZY_{Mo} and ZSM5_{Mo}), whereas the band at 991 cm^{-1} was shifted to lower wavenumbers. These changes were less evident in the ZSM5 zeolites due to their very small Mo content (Tables 4 and 5). It should be noted that the spectra of different samples from different preparations were very reproducible.

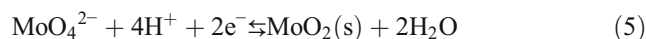
In summary, the characterization of the modified zeolites evidences the presence in them of Co, Mo, or both. In all cases, the metals were mostly, if not exclusively, on the outer surface of the zeolites. Mo did form grains on the outer surface of ZA_{Mo} , and needles on the outer surface of ZY_{Mo} and ZSM5_{Mo} . Probably, the grains were orthorhombic $\alpha\text{-MoO}_3$, and the needles *hex*- MoO_3 . These grains and needles could be

largely eliminated by washing with hot water, as confirmed by XPS, FTIR spectroscopy, and EDS. As reported by Debecker et al. [19, 24] for Mo species supported on mesoporous silica–alumina, the $\text{Mo}_7\text{O}_{24}^{6-}$ anion interacts strongly with the Al centers on the surface of the support, which facilitates the dispersion of the Mo. The different structures of the MoO_3 forming the new phases observed in the SEM micrographs should be related to the different proportions of Al and Si centers on the zeolite surfaces, which would lead to the nucleation of different structures of the same compound.

Cyclic Voltammetry of GC/Graphite-Modified Zeolite Electrodes in a pH 3 Electrolyte

We carried out preliminary CVs of the Mo-modified zeolites at pH 3, 7, and 9. The best results were obtained at pH 3, because at this pH both Mo(VI) and Mo(IV) form insoluble species, MoO_3 and MoO_2 , respectively, which improves the stability of the electrodes [20, 51]. All the CVs in Fig. 6 were carried out at 0.02 V s^{-1} starting from the rest potential, indicated by the vertical arrows, toward negative potentials. Two CVs (between -0.81 and $1.24 \text{ V}_{\text{RHE}}$ and between -0.6 and $0.8 \text{ V}_{\text{RHE}}$) of a GC/graphite electrode in a pH 3 solution of

$0.1 \text{ mol L}^{-1} \text{ Na}_2\text{SO}_4$ plus $1 \text{ mmol L}^{-1} (\text{NH}_4)_6\text{Mo}_7\text{O}_{24}$ (Fig. 6—graphite) showed, independently of potential limits, only a redox couple, c1/a1, with peak potentials of -0.14 and $0.22 \text{ V}_{\text{RHE}}$, respectively. This process probably corresponds to the reaction



whose redox potential is a matter of discussion [52–54]. A pair of peaks at about -0.4 and -0.3 V vs Ag/AgCl was found by Jońca et al. [53] in CVs of a gold disc in 0.6 M NaCl solutions of both pH 2.04 and 1.42 containing sodium molybdate.

The CVs between -0.61 and $1.24 \text{ V}_{\text{RHE}}$ in a pH 3 solution of $0.1 \text{ mol L}^{-1} \text{ Na}_2\text{SO}_4$ of GC/g-Z electrodes (curves 1), GC/g- Z_{Mo} electrodes both as prepared (curves 2), and after washing with hot water (curves 3), for ZA, ZY, and ZSM5 are given in Fig. 6. The three unmodified GC/g-Z electrodes (curves 1 in Fig. 6) showed the well-known flat CV [21] and a wide, nearly negligible couple near $0.64 \text{ V}_{\text{RHE}}$ associated with the C–OH/C=O process of the graphite carbonyl groups. The three Mo-modified zeolites showed (curves 2 in Fig. 6) five clearly defined pairs of peaks, which is most interesting, since the multiplicity of voltammetric peaks is nearly a hallmark of polyoxometallates, which in this case have been obtained simply by impregnation of zeolites with a molybdate solution. The first pair of peaks had a half-sum potential of about $-0.1 \text{ V}_{\text{RHE}}$, which is about 0.1 V more negative than the half-sum potential of $+0.035 \text{ V}_{\text{RHE}}$ of the a1/c1 pair of the $\text{Mo}_7\text{O}_{24}^{6-}$ anion on GC/g (Fig. 6—graphite), and therefore, should correspond to a different process. These results clearly show that the Mo compound responsible for the five pairs of voltammetric peaks of ZA and ZSM5 forms only on zeolites, but not on a GC/graphite electrode.

The CVs of the three Mo-modified zeolites after washing with hot water (curves 3 in Fig. 6) show that while in the case of ZA the CV remains practically the same (curve 3 in Fig. 6—ZA), in the case of GC/g- ZY_{Mo} (curve 3 in Fig. 6—ZY), the peaks decreased only slightly, and in GC/g- ZSM5_{Mo} (curve 3 in Fig. 6—ZSM5) decreased very much but could still be seen. Therefore, the Mo compound responsible for the multiplicity of peaks is not present in the needles on the outer surface of the zeolites, since these peaks remain after washing away the needles with hot water. We suggest that the electrochemically active compound was the $\text{Mo}_7\text{O}_{24}^{6-}$ isopolyoxomolybdate anion, proceeding from the impregnation solution and anchored on the zeolite surface, perhaps by a strong interaction with its acidic sites.

Pourbeyram et al. [30] observed three pairs of peaks in CVs on GC of a heteropolyoxometalate, phosphomolybdic acid ($\text{H}_3\text{PMo}_{12}\text{O}_{40}$), in $0.1 \text{ M H}_2\text{SO}_4$. Three pairs of peaks also appeared when the phosphomolybdic acid was dispersed within dealuminated ZY zeolite, but they were negatively shifted by about 0.5 – 0.7 V . Zhao et al. [50] synthesized a

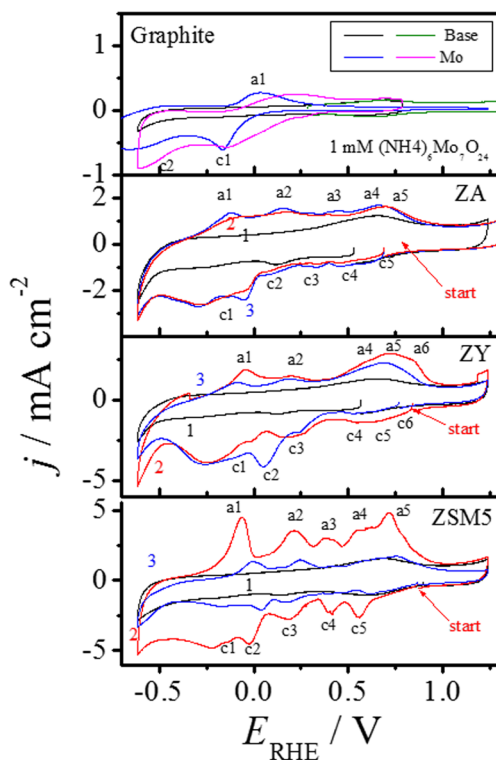


Fig. 6 Cyclic voltammograms at 0.02 V s^{-1} in a deaerated pH 3, $0.1 \text{ M Na}_2\text{SO}_4$ solution of (a) GC/graphite electrode in the pH 3 base electrolyte and in the presence of $1 \text{ mM } (\text{NH}_4)_6\text{Mo}_7\text{O}_{24}$. Introduce ZA GC/graphite- $\text{Z}_{\text{A}_{\text{Mo}}}$ electrode. Introduce ZB GC/graphite- ZY_{Mo} electrode. Introduce ZSM5 GC/graphite- ZSM5_{Mo} electrode. Curves 1: GC/graphite-Z electrode; curves 2: GC/graphite- Z_{Mo} ; and curves 3: GC/graphite- Z_{Mo} after washing in hot water. Zeolite loading 3.3 mg Z/cm^2 , $R_f = 136 \pm 18$

Keggin-type isopolyoxometallate, $[(C_3H_5N_2)_4H[Mo^{VI}_{0.5}Mo^{VI}_{12}O_{40}]]$, which showed four pairs of peaks in CVs in DMF.

Assuming that each pair of peaks corresponds to a 2-electron process, we estimated the amount of Mo electrochemically active sites by integrating the charge of the anodic region between about -0.25 and $0.9 V_{RHE}$ of the modified zeolites (curves 2 in Fig. 6—ZA, ZY, and ZSM5) and subtracting the electrical charge of the respective unmodified zeolites (curves 1 in the same figures). The estimated Mo amount was 0.09 , 0.11 , and $0.24 \mu\text{mol cm}^{-2}$ (geo) for the ZA, ZY, and ZSM5 zeolites, respectively (Table 5). Washing with hot water decreased the amount of Mo (curves 3 in Fig. 6—ZA, ZY, and ZSM5), the remaining Mo being 89% in ZA, 56% in ZY, and 26% in ZSM5. It is very interesting that ZA, the more hydrophilic zeolite, had the lowest Mo loading, but this Mo was strongly anchored on the surface, because it remained practically to the same extent after hot-water washing, as can be seen by the near coincidence of the respective CVs in Fig. 6—ZA. On the contrary, the more hydrophobic zeolite, ZSM5, had the highest Mo loading, but this Mo was anchored rather weakly, the CV after the washing barely emerging from that of the unmodified zeolite, as can be seen in Fig. 6—ZSM5.

Active molybdenum loading, half-sum potentials, and peak separation of the redox couples obtained from cyclic voltammograms at $0.02 V s^{-1}$ in a pH 3 solution of glassy carbon electrodes modified with a mixture of graphite and molybdenum-modified zeolites are given in Table 5. The half-sum potentials, that is, half the sum of the anodic and cathodic peak potentials, constitute a good approximation to the reversible potentials and are very similar for peaks 1, 2, 3, and 5 in ZA_{Mo} and $ZSM5_{Mo}$ (peak 4 is missing in ZA_{Mo}). However, while the peak separation of the five redox processes of the $ZSM5_{Mo}$ zeolite is 130 – 200 mV, indicating that these processes are very irreversible, the five redox processes of the ZA_{Mo} zeolite are less irreversible, with a peak separation of only about 70 mV.

The Mo-based electrodes were stable, because repetitive CVs of them showed no significant changes (Fig. S5).

The CVs of Co-exchanged zeolites coincide with those of the unexchanged zeolites (Fig. S6), showing that the Co present had no electrochemical activity. And, as was to be expected, the CVs of the electrodes modified with both Co and Mo coincided with those of Mo-modified zeolites (Fig. S6).

Oxygen Reduction Reaction

Cyclic Voltammetry of the Electroreduction of Oxygen

The CVs at $0.02 V s^{-1}$, starting negatively from the open circuit potential down to $-0.61 V_{RHE}$ and then up to $1.2 V_{RHE}$, in an O_2 -saturated $0.1 \text{ mol L}^{-1} Na_2SO_4$ solution

of pH 3, using GC/g-Z electrodes (curves 1) and GC/g- ZCo (curves 2), GC/g- Z_{Mo} (curves 3), and GC/g- $ZCoMo$ (curves 4) electrodes for ZA, ZY, and ZSM5, are shown in Fig. 7. The oxygen reduction peak (peak 1C) appeared at about $0.1 V_{RHE}$ in all the electrodes. Oxygen shifts negatively the hydrogen evolution, which affects the Mo(VI)/Mo(IV) peak potentials, and therefore, some small Mo peaks appear in the CVs of the Mo- and Co-Mo-modified zeolites. The current density of peak 1C was almost the same, 10 mA cm^{-2} , for the Mo-modified ZA and ZY zeolites, which was about twice that for the unmodified zeolites, clearly showing the catalytic activity of Mo for the ORR. Surprisingly, the current density of the very sharp peak 1C of the unmodified ZSM5 zeolite was very high, 22 mA cm^{-2} , and about the same for Co-Mo-modified ZSM5 (Fig. 7—ZSM5). Possibly, the hydrophobic character of this zeolite favors the access of oxygen to the electrode surface by weakening the binding of water to the zeolite surface. The high value of the peak current density with Co-Mo-modified ZSM5 could be due to the fact that this peak was very sharp, the current at more negative potentials decreasing so steeply that at $-0.25 V$ it had decreased so much that it was comparable with those of the ZA- and ZY-based electrodes.

As said above, although washing with hot water eliminated most of the Mo-containing grains from the outer surface of the ZA zeolite, its CV retained the five pairs of peaks (Fig. S7a). As can be seen in the CV at $0.02 V s^{-1}$ in Fig. S7b, the current for the ORR of a Mo-modified ZA electrode was practically unaffected if the zeolite was previously washed with hot water, which shows that the Mo-containing grains had no significant activity for the ORR.

As can be seen in Fig. S8, dissolved heptamolybdate inhibits the ORR and probably the hydrogen evolution as well. Since our electrodes were active for the ORR, it is clear that desorption of the heptamolybdate adsorbed on the zeolite surface was negligible.

Linear Potential Sweeps in the Kinetically Controlled Region of the ORR

The graphite-zeolite electrodes had high capacitive currents in CVs at $0.02 V s^{-1}$ (Fig. 7), as was to be expected from their high roughness factor, 131 ± 5 . However, these capacitive currents became negligible when the scan rate was reduced to $0.002 V s^{-1}$, at which the kinetic measurements were carried out. The LPS under magnetic electrolyte stirring at $0.002 V s^{-1}$ in an O_2 -saturated $0.1 \text{ mol L}^{-1} Na_2SO_4$ solution of pH 3 electrolyte of electrodes based on ZA, ZY, and ZSM5, after subtraction of the capacitive current, is shown in Fig. 8. In the case of ZA and ZY, the currents tend to plateau off at about $0.15 V$, at which potential the diffusion limit is reached, while with ZSM5, there appears a peak at this potential. At more negative potentials, a well-defined plateau was reached, except for the GC/g and GC/g-Z electrodes. The onset

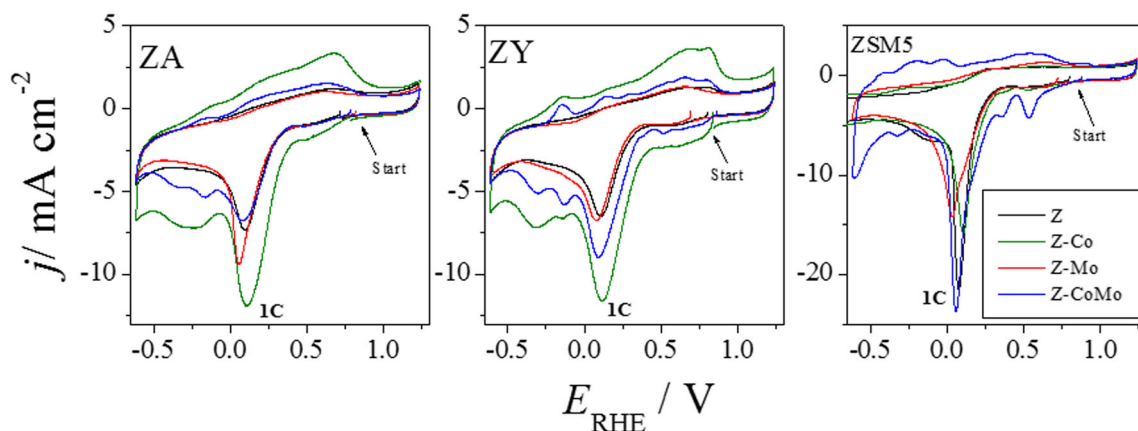


Fig. 7 Cyclic voltammograms at 0.02 V s^{-1} in an O_2 -saturated pH 3, 0.1-M Na_2SO_4 electrolyte, of the following electrodes: GC/graphite-unmodified zeolite and GC/graphite- Z_M electrodes, where M is Co, Mo, and Co–Mo. Zeolite loading 3.3 mg Z/cm^2 , $R_F = 131 \pm 5$

potentials, evaluated as the intersection with the potential axis of the extrapolation of the linear section of the current–potential curves in Fig. 8, are given in Table 6. In all cases, the onset potentials with untreated and metal-modified zeolites were about 0.1 V more positive than that of 0.30 V for the GC/graphite electrode, a modest activity increase. Clearly, the highest onset potentials, 0.41–0.42 V, were those obtained with the ZA_{Co} and ZY_{Co} electrodes.

As was the case with the CVs, the LPS for the ORR of the GC/g- ZA_{Mo} electrode remained practically the same if the zeolite was previously washed with hot water (Fig. S9), which again shows that the Mo-containing particles on the surface of the unwashed zeolite had no significant activity for the ORR.

The Tafel plots of the ORR on the different electrodes, obtained from the curves in Fig. 8, are given in Fig. 9 and the corresponding Tafel slopes in Table 6. The Tafel slope of the ORR with a GC/g electrode was about $0.120 \text{ V decade}^{-1}$.

The Tafel slopes with GC/g-Z electrodes were somewhat higher, which cannot be due to an increase of the electrode resistance caused by the insulating zeolites, since this ohmic effect would obviously be linear with the potential.

The graphite/unmodified zeolites (Fig. 9) modestly decreased the overpotential of the ORR at $56 \mu\text{A cm}^{-2}$ by 83 (ZA), 111 (ZY), and 62 (ZSM5) mV as compared with that of GC/graphite electrodes. This decrease was significantly greater, 112 and 146 mV, for electrodes based on ZA_{Co} and ZY_{Co} , respectively, but about the same for ZSM5_{Co} . The modification with Mo increased the overpotential in the case of ZA, did not change it in ZY, and decreased it slightly in ZSM5, with respect to the unmodified zeolites. And the modification with both Co and Mo decreased slightly the overpotential only in the case of ZSM5. For ZSM5, the Tafel plots of the Co-modified, the Mo-modified, and the Co- and Mo-modified zeolite nearly coincide (Fig. 9), which should be due to the negligible

Fig. 8 Linear potential sweeps at 0.002 V s^{-1} in an O_2 -saturated pH 3, 0.1-M Na_2SO_4 electrolyte, of the following electrodes: GC/graphite, GC/graphite-Z, and GC/graphite- Z_M electrodes, where M is Co, Mo, and Co–Mo. Zeolite loading 3.3 mg Z/cm^2 , $R_F = 131 \pm 5$

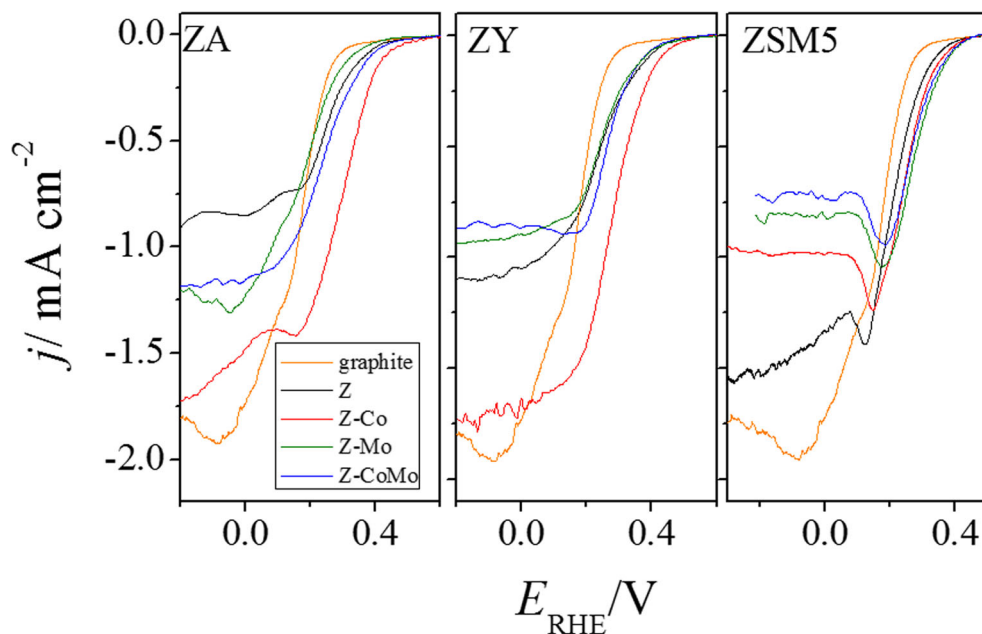


Table 6 Onset potentials and Tafel slopes of the ORR obtained from Fig. 8. The percentage of H₂O₂ yield at -0.2 and -0.1 V_{RHE} determined by RRDE experiments at 1600 rpm was obtained from Fig. 10 for the ZA-based electrodes (the plots for the ZY- and ZSM5-based electrodes are not shown)

Electrode	Onset potential/V vs RHE	Tafel slope/V decade ⁻¹	% of H ₂ O ₂ as evaluated with Eq. (6)	
			$E = -0.2$ V	$E = -0.1$ V
GC/graphite	0.28	-0.115 ± 0.001	2.8	3.0
GC/graphite-ZA	0.35	-0.187 ± 0.002	2.0	2.2
GC/graphite-ZA _{Co}	0.42	-0.146 ± 0.001	10.0	10.7
GC/graphite-ZA _{Mo}	0.32	-0.170 ± 0.001	5.6	4.7
GC/graphite-ZA _{CoMo}	0.37	-0.175 ± 0.001	12.7	11.5
GC/graphite-ZY	0.34	-0.184 ± 0.003	1.1	1.3
GC/graphite-ZY _{Co}	0.41	-0.143 ± 0.002	0.0	0.0
GC/graphite-ZY _{Mo}	0.36	-0.185 ± 0.002	0.36	0.42
GC/graphite-ZY _{CoMo}	0.35	-0.150 ± 0.001	0	0
GC/graphite-ZSM5	0.33	-0.118 ± 0.001	0.10	0.16
GC/graphite-ZSM5 _{Co}	0.34	-0.121 ± 0.001	0.13	0.24
GC/graphite-ZSM5 _{Mo}	0.36	-0.119 ± 0.002	0.84	1.02
GC/graphite-ZSM5 _{CoMo}	0.37	-0.134 ± 0.002	0	0

exchange capacity of this zeolite, more than to its hydrophobic character. Summing up, only the Co-modified ZA and ZY electrodes had significantly lower overpotentials for the ORR than the unmodified zeolite electrodes. However, these overvoltage decreases are of little practical significance, since they are compensated for by the considerable increase of the Tafel slope.

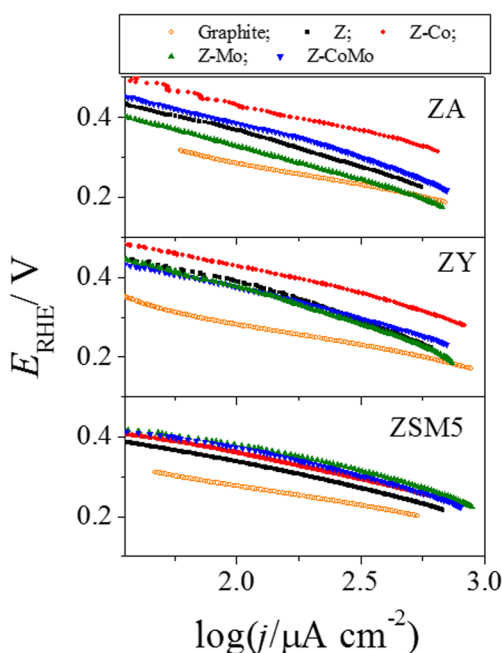


Fig. 9 Tafel plots in the kinetic region of the beginning of the oxygen reduction as obtained from the linear potential sweeps at 0.002 V s⁻¹ in an O₂-saturated pH 3, 0.1-M Na₂SO₄ electrolyte in Fig. 8. The electrodes were GC/graphite, GC/graphite-Z, and GC/graphite-Z_M, where M is Co, Mo, and Co-Mo. Zeolite loading 3.3 mg Z/cm²

Hydrogen Peroxide Detection with Au Ring/(GC/g-Z) Disc Electrodes

In order to detect the hydrogen peroxide, a gold ring-(GC/g-Z_M) disc rotating electrode was used. The collection factor, N ($N = I_R/I_D$), was determined using 2 mmol L⁻¹ Fe(CN)₆³⁻ in 1 mol L⁻¹ KNO₃ [55]. The gold ring was held at a potential of 1.3 V vs the RHE. The disc (bottom plots) and ring (upper plots) currents for unmodified and modified ZA-based electrodes in negative-going LPSs are shown in Fig. 10, and the efficiencies for H₂O₂ production at a disc potential of -0.20 and -0.1 V vs RHE and 1600 rpm are given in Table 6. The efficiency for H₂O₂ production was evaluated as $p \times 100$, the parameter p being [56]:

$$p = 2x \frac{I_R}{I_D + \frac{I_R}{N}} \quad (6)$$

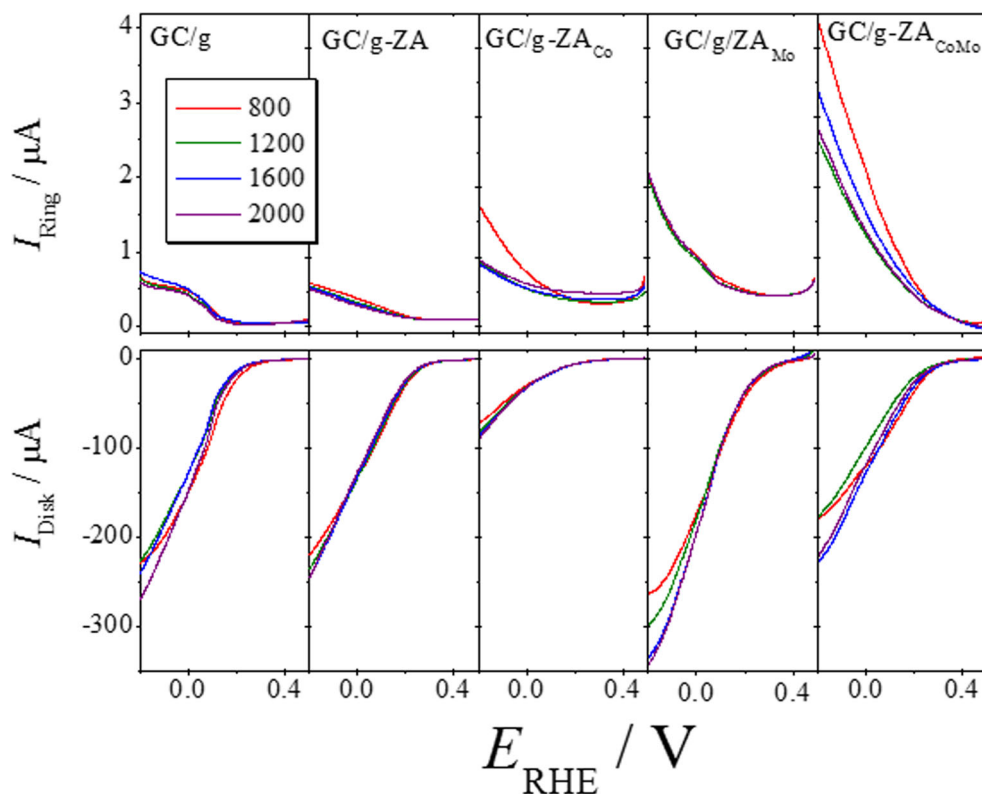
Where I_R : ring current density, I_D : disc current density, and N : collection factor. The total number of electrons transferred per O₂ molecule is [56]:

$$n = 4 - 2p \quad (7)$$

The value of n was nearly 4 for almost all the electrodes, evidencing a low performance for the production of hydrogen peroxide.

The efficiency of GC/graphite at a disc potential of -0.2 V_{RHE} was 2.8%. The efficiency with GC/graphite-ZA_{Mo} was twice higher, with GC/graphite-ZA_{Co} 3.6 times higher, and with GC/graphite-ZA_{CoMo} 4.5 times higher.

Fig. 10 Linear potential sweeps at 0.002 V s^{-1} of the gold ring currents (upper plots) and of the GC/graphite-ZA disc currents (bottom plots) of an RRDE in O_2 -saturated pH 3 electrolyte at different rotation rates. Zeolite loading 1.83 mg Z/cm^2 , $R_f = 11.0 \pm 0.5$



All the ZY- and ZSM5-containing electrodes showed very poor efficiencies for H_2O_2 production, none of them reaching the 1% level (Table 6). However, as will be shown below, in long-term electrolyses, the highest H_2O_2 concentrations were obtained with the Mo-modified zeolites, this yield being practically the same for the three zeolites and about 5 times higher than the concentrations obtained with the GC/graphite electrodes.

Hydrogen Peroxide Production in Long-Time Electrolyses

In order to determine the stability of the electrodes, 4-h electrolyses at $-0.2 \text{ V}_{\text{RHE}}$ of O_2 -saturated $0.1 \text{ mol L}^{-1} \text{ Na}_2\text{SO}_4$ solutions of pH 3 were carried out. Samples were taken at regular intervals, and their hydrogen peroxide concentration was determined by UV–vis spectroscopy of the colored complex with TiO_2^+ [28, 29], using the equation:

$$\text{Absorbance} = -(0.001 \pm 0.0018) + (0.7510 \pm 0.0074) [\text{H}_2\text{O}_2] \quad (8)$$

The evolution of the concentration of hydrogen peroxide is shown in Fig. 11 for ZA, ZY, and ZSM5. The three zeolites modified only with Mo yielded the highest H_2O_2 concentrations, which, again, we attribute to the presence of the $\text{Mo}_7\text{O}_{24}^{6-}$ isopolyoxomolybdate on the surface of the zeolites.

The unmodified ZA and ZY zeolites had H_2O_2 yields only slightly higher than that of graphite, while the unmodified

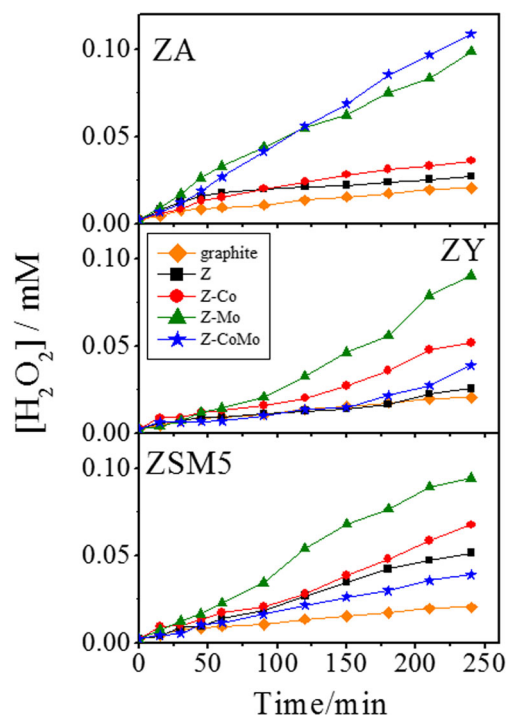


Fig. 11 Evolution of the hydrogen peroxide concentration during 4-h electrolyses at -0.2 V in an O_2 -saturated pH 3, $0.1\text{-M Na}_2\text{SO}_4$ solution using GC/graphite–zeolite electrodes, and GC/g- Z_M electrodes, where M is Co, Mo, and Co–Mo. Zeolite loading 2.0 mg Z/cm^2

ZSM5 had a rather high yield, about half that of the Mo-modified zeolite. This agrees with the high peak current density (Fig. 7—ZSM5) and the high kinetic current density (Fig. 8—ZSM5) for the ORR of unmodified ZSM5. Co exchange did not significantly improve the H_2O_2 yield of ZA (Fig. 11—ZA), but it did so for ZY and ZSM5. And while for ZA the exchange with both Co and Mo slightly improved the yield over that with Mo alone, for ZY and ZSM5, the yield with both Co and Mo was very low, only slightly higher than that with graphite alone. The Co on the 3-nm surface layer, as determined by XPS, was low for the three zeolites.

The fact that for all the Mo-modified zeolite electrodes the hydrogen peroxide concentration increased at a rather steady rate over the 4-h electrolysis shows that these electrodes are stable and that, therefore, they could be interesting for the degradation of pesticides by a Fenton-like process.

The stark difference between the efficiencies for H_2O_2 production determined in RRDE experiments and in long-time electrolyses is due to the fact that the H_2O_2 yield of Co-modified electrodes decreased with time. This can be clearly seen in Fig. 11, which shows that although initially the H_2O_2 yield was higher for the ZY- and ZSM5-based Co-modified electrodes, soon the Mo-modified electrodes took the lead. We assume that this is due to a loss of Co in the Co-modified electrodes during the ORR.

Conclusions

Cobalt can be exchanged with the zeolite cations, while molybdenum cannot, because at the pH 3 used here it cannot form cationic species. Furthermore, in the case of ZSM5, practically no cation exchange can take place, since its Al/Si ratio, which determines its maximum possible exchanged cation/Si ratio, is only 0.02. A Mo compound, most probably an oxide, was deposited on the surface of the zeolites, as attested by the SEM-EDS, XRD, FTIR-ATR, and XPS analyses. Probably, this oxide was MoO_3 , as grains (rhombic MoO_3) in ZA and as needles (hexagonal MoO_3) in ZY and ZSM5. After washing with hot water, some grains remained in ZA, while the needles in ZY and ZSM5 were largely washed away. Very interestingly, the CVs of the Mo-modified zeolites showed five clearly defined pairs of peaks in the case of ZA and ZSM5 and possibly six pairs in ZY. This points to the presence on the outer surface of the zeolites of the adsorbed $\text{Mo}_7\text{O}_{24}^{6-}$ isopolyoxomolybdate anion, proceeding from the impregnating solution. Currently, the electrochemistry of polyoxomolybdates is being actively investigated, both from the basic and applied fields, the latter because of their possible use in electrocatalysis. With respect to Co, the XPS results show that in three zeolites, the Co is in a similar structure, mainly as a Co^{2+} species similar to those of Co in ion-exchange sites in zeolites.

The ORR currents in the kinetic range of the three graphite/unmodified zeolite electrodes were higher than those with graphite alone. Only the modification with Co of the ZA and ZY zeolites, but not that with Mo or Co-Mo in all the other cases, significantly improved these currents and therefore modestly decreased the overpotential. Unfortunately, the considerable increase of the Tafel slopes of the modified zeolites ran counter to their overpotential decreases.

In long-time electrolyses, the three Mo-modified zeolites modified generated a hydrogen peroxide concentration high enough for pesticide degradation. This concentration was the same for the three zeolites, irrespective of their exchange capacity and their hydrophobic/hydrophilic character. Initially, the H_2O_2 yield was the highest for the Co-modified electrodes, but this yield decreased with time, which we assume was due to a loss of Co during the ORR. The rotating ring-disc experiments gave only short-time results, which were shown to be not applicable to a possible industrial use.

Funding Information This work was supported by CONICYT Chile under Grant FONDECYT-1140207 and FONDEQUIP-EQM 160070 and DICYT-USACH grant 021841UZ. FF acknowledges a MECESUP USA 1555 Grant.

References

1. I. Sirés, E. Brillas, M.A. Oturan, M.A. Rodrigo, M. Panizza, Electrochemical advanced oxidation processes: today and tomorrow. A review. *Sci. Pollut. Res.* **21**(14), 8336–8367 (2014)
2. E.G. Garrido-Ramírez, M.L. Mora, J.F. Marco, M.S. Ureta-Zañartu, Characterization of nanostructured allophane clays and their use as support of iron species in a heterogeneous electro-Fenton system. *Appl. Clay Sc.* **86**, 153–161 (2013)
3. E.G. Garrido-Ramírez, J.F. Marco, N. Escalona, M.S. Ureta-Zañartu, Preparation and characterization of bimetallic Fe-Cu allophane nanoclays and their activity in the phenol oxidation by heterogeneous electro-Fenton reaction. *Micropor. Mesopor. Mat.* **225**, 303–311 (2016)
4. G. Santana-Martínez, G. Roa-Morales, E.M. Del Campo, R. Romero, B.A. Frontana-Urbe, R. Natividad, Electro-Fenton and electro-Fenton-like with in situ electrogeneration of H_2O_2 and catalyst applied to 4-chlorophenol mineralization. *Electrochim. Acta* **195**, 246 (2016)
5. A. Doménech-Carbó, Theoretical scenarios for the electrochemistry of porous silicate-based materials: an overview. *J. Solid State Electrochem.* **19**(7), 1887–1903 (2015)
6. C. Baerlocher, L.B. McCusker, D.H. Olson, *Atlas of Zeolites Framework Types*, 6th edn. (Elsevier, Amsterdam, 2007)
7. D.R. Rolison, C. Bessel, Electrocatalysis and charge-transfer reactions at redox-modified zeolites. *Acc. Chem. Res.* **33**, 737 (2000)
8. A. Walcarius, Electroanalytical applications of microporous zeolites and mesoporous (organo)silicas: recent trends. *Electroanalysis* **20**(7), 711–738 (2008)
9. D. Rolison, Zeolite-modified electrodes and electrode-modified zeolites. *Chem. Rev.* **90**(5), 867–878 (1990)
10. Z. Mojović, P. Banković, Ć.N. Jović-Jovići, A. Milutinović-Nikolić, A. Rabi-Stanković, D. Jovanović, Electrocatalytic behavior of nickel impregnated zeolite electrode. *Int. J. Hydrog. Energy* **36**, 13343 (2011)

11. J.B. Raoof, N. Azizi, R. Ojani, S. Ghodrati, M. Abrishamkar, F. Chekin, Synthesis of ZSM-5 zeolite: electrochemical behavior of carbon paste electrode modified with Ni(II)-zeolite and its application for electrocatalytic oxidation of methanol. *Int. J. Hydrog. Energy* **36**(20), 13295–13300 (2011)
12. A.A. El-Shafei, A. Alakl, A.M. Ouf, Preparation, characterization and electrochemical behavior of Pd-Au alloy incorporated into zeolites/graphite electrodes. *Electroanalysis* **26**(8), 1810–1815 (2014)
13. A. Satsuma, D. Yang, K.I. Shimizu, Effect of acidity and pore diameter of zeolites on detection of base molecules by zeolite thick film sensor. *Micropor. Mesopor. Mater.* **141**(1–3), 20–25 (2011)
14. S.N. Azizi, S. Ghasemi, M. Mikhchian, Microwave-assisted synthesis of NaA nanozeolite from slag and performance of Ag-doped nanozeolite as an efficient material for determination of hydrogen peroxide. *RSC Adv.* **6**(57), 52058–52066 (2016)
15. Z. Moiovich, L. Iovanovich, S. Mentus, D. Iovanovich, Reduction of oxygen at a NaX–Ag composite electrode and its application to the determination of oxygen in aqueous media. *J. Anal. Chem.* **65**(1), 77–81 (2010)
16. J.F. Carneiro, L.C. Trevelin, A.S. Lima, G.N. Meloni, M. Bertotti, P. Hammer, R. Bertazzoli, M.R.V. Lanza, Synthesis and characterization of ZrO₂/C as electrocatalyst for oxygen reduction to H₂O₂. *Electrocatalysis* **8**(3), 189–195 (2017)
17. M.Z. Iqbal, R.J. Kriek, Silver/nickel oxide (Ag/NiO) nanocomposites produced via a citrate sol-gel route as electrocatalyst for the oxygen evolution reaction (OER) in alkaline media. *Electrocatalysis* **9**(3), 279–286 (2018)
18. O.M. Ama, N. Kumar, F.V. Adams, S.S. Ray, Efficient and cost-effective photoelectrochemical degradation of dyes in wastewater over an exfoliated graphite–MoO₃ nanocomposite electrode. *Electrocatalysis* **9**(5), 623–631 (2018). <https://doi.org/10.1007/s12678-018-0471-5>
19. D.P. Debecker, M. Stoyanova, U. Rodemerck, E.M. Gaigneaux, Preparation of MoO₃/SiO₂–Al₂O₃ metathesis catalysts via wet impregnation with different Mo precursors. *J. Mol. Catal. A Chem.* **340**(1–2), 65–76 (2011)
20. V.S. Saji, C.W. Lee, Molybdenum, molybdenum oxides, and their electrochemistry. *ChemSusChem* **5**(7), 1146–1161 (2012)
21. F. Fernández, C. Berrios, E. Garrido-Ramírez, N. Escalona, C. Gutiérrez, M.S. Ureta-Zañartu, Electrooxidation of 2-chlorophenol and 2,4,6-chlorophenol on glassy carbon electrodes modified with graphite–zeolite mixtures. *J. Appl. Electrochem.* **44**(1295) (2014)
22. K. Kodama, A. Beniya, N. Isomura, Y. Watanabe, Electrochemical observation of high oxophilicity and its effect on oxygen reduction reaction activity of Au clusters mass-selectively deposited on glassy carbon. *Electrocatalysis* **9**(4), 471–479 (2018)
23. M. Mhamdi, S. Khaddar-Zine, A. Ghorbel, Influence of the cobalt salt precursors on the cobalt speciation and catalytic properties of H-ZSM-5 modified with cobalt by solid-state ion exchange reaction. *Appl. Catal. A Gen.* **357**(1), 42–50 (2009)
24. D.P. Debecker, M. Stoyanova, U. Rodemerck, A. Léonard, B.L. Su, E.M. Gaigneaux, Genesis of active and inactive species during the preparation of MoO₃/SiO₂–Al₂O₃ metathesis catalysts via wet impregnation. *Catal. Today* **169**(1), 60–68 (2011)
25. J.J. Cruywagen, A.G. Draaijer, J.B.B. Heyns, E.A. Rohwer, Molybdenum(VI) equilibria in different ionic media. Formation constants and thermodynamic quantities. *Inorg. Chim. Acta* **331**(1), 322–329 (2002)
26. J.J. Cruywagen, Protonation, oligomerization, and condensation reactions of vanadate(V), molybdate(VI), and tungstate(VI). *Adv. Inorg. Chem.* **49**, 127 (1999)
27. M. Mohai, XPS MultiQuant: multimodel XPS quantification software. *Surf. Interface Anal.* **36**(8), 828–832 (2004)
28. F.J. Welcher, *Standard Methods of Chemical Analysis*. 6th ed, Vol. 2 (Part B) (Krieger RE Pub Co, New York, 1975) pp 1827
29. K. Kosaka, H. Yamada, S. Matsui, S. Echigo, K. Shishida, Comparison among the methods for hydrogen peroxide measurements to evaluate advanced oxidation processes: application of a spectrophotometric method using copper(II) ion and 2,9-dimethyl-1,10-phenanthroline. *Environ. Sci. Technol. Lett.* **38**(11), 3821–3824, 32 (1998)
30. S. Pourbeyram, M. Moosavifar, V. Hasanzadeh, Electrochemical characterization of the encapsulated polyoxometalates (POMs) into the zeolite. *J. Electroanal. Chem.* **714–715**, 19 (2014)
31. M.H. Tran, H. Ohkita, T. Mizushima, N. Kakuta, Hydrothermal synthesis of molybdenum oxide catalyst: heteropoly acids engaged in US-Y. *Appl. Catal. A Gen.* **287**(1), 129–134 (2005)
32. M.M.J. Treacy, J.B. Higgins, *Collection of Simulated XRD Powder Patterns for Zeolites*. Published on behalf of the Structure Commission of the International Zeolite Association, 4th ed (Elsevier, Oxford, 2001) p 250
33. K.B. Klepper, O. Nilsen, H. Fjellvåg, Epitaxial growth of cobalt oxide by atomic layer deposition. *J. Crystal. Growth* **307**(2), 457–465 (2007)
34. W. Yuan, J. Zhang, D. Xie, Z. Dong, Q. Su, G. Du, Porous CoO/C polyhedra as anode material for Li-ion batteries. *Electrochim. Acta* **108**, 506–511 (2013)
35. W. Pan, R. Tian, H. Jin, Y. Guo, L. Zhang, X. Wu, L. Zhang, Z. Han, G. Liu, J. Li, G. Rao, H. Wang, W. Chu, Structure, optical, and catalytic properties of novel hexagonal metastable h-MoO₃ nano- and microrods synthesized with modified liquid-phase processes. *Chem. Mater.* **22**, 6202 (2010)
36. J. Song, X. Ni, L. Gao, H. Zheng, Synthesis of metastable h-MoO₃ by simple chemical precipitation. *Mater. Chem. Phys.* **102**(2–3), 245–248 (2007)
37. J. Zhou, N. Lin, L. Wang, K. Zhang, Y. Zhou, Y. Qian, Synthesis of hexagonal MoO₃ nanorods and their electrochemical performance as anode materials for lithium-ion battery. *J. Mat. Chem.* **A3**(7463) (2015)
38. M. Gracia, J.F. Marco, J.R. Gancedo, W. Exel, W. Meisel, Surface spectroscopic study of the corrosion of ultrathin 57Fe-evaporated and Langmuir-Blodgett films in humid SO₂ environments. *Surf. Interf. Anal.* **29**, 82 (2000)
39. J.F. Marco, J.R. Gancedo, J. Ortiz, J.L. Gautier, Characterization of the spinel-related oxides Ni_xCo_{3-x}O₄ (x=0.3,1.3,1.8) prepared by spray pyrolysis at 350 °C. *Appl. Surf. Sci.* **227**, 175 (2004)
40. C. Chupin, A.C. van Veen, M. Konduru, J. Després, C. Mirodatos, Identity and location of active species for NO reduction by CH₄ over Co-ZSM-5. *J. Catal.* **241**, 103 (2006)
41. Q. Tang, Q. Zhang, P. Wang, Y. Wang, H. Wan, Characterizations of cobalt oxide nanoparticles within Faujasite zeolites and the formation of metallic cobalt. *Chem. Mater.* **16**(10), 1967–1976 (2004)
42. Y. Zhou, Q. Liu, D. Liu, H. Xie, G. Wu, W. Huang, Y. Tian, Q. He, A. Khalil, Y.A. Haleem, T. Xiang, W. Chu, C. Zou, L. Song, Carbon-coated MoO₂ dispersed in three-dimensional graphene aerogel for lithium-ion battery. *Electrochim. Acta* **174**, 8–14 (2015)
43. J. Baltrusaitis, B. Mendoza-Sanchez, V. Fernández, R. Veenstra, N. Dukstiene, A. Roberts, N. Fairley, Generalized molybdenum oxide surface chemical state XPS determination via informed amorphous sample model. *Appl. Surf. Sci.* **326**, 151–161 (2015)
44. V. Crupi, D. Majolino, F. Longo, P. Migliardo, V. Venuti, FTIR/ATR study of water encapsulated in Na-A and Mg-exchanged A-zeolites. *Vib. Spectrosc.* **42**(2), 375–380 (2006)
45. L. Ohlin, P. Bazin, F. Thibault-Starzyk, J. Hedlund, M. Grahn, Adsorption of CO₂, CH₄, and H₂O in zeolite ZSM-5 studied using *in situ* ATR-FTIR spectroscopy. *J. Phys. Chem. C* **117**, 16972 (2013)

46. T. Montanari, O. Marie, M. Daturi, G. Busca, Cobalt on and in zeolites and silica–alumina: spectroscopic characterization and reactivity. *Catal. Today* **110**(3–4), 339–344 (2005)
47. F. Geobaldo, B. Onida, P. Rivolo, F. Di Renzo, F. Fajula, E. Garrone, *Catal. Today* **70**, 107 (2001)
48. G. Li, FT-IR studies of zeolite materials: characterization and environmental applications. PhD thesis, University of Iowa, [http://ir.uiowa.edu/etd/96\(2005\)](http://ir.uiowa.edu/etd/96(2005))
49. D.H. Olson, The crystal structure of dehydrated NaX. *Zeolites* **15**(5), 439–443 (1995)
50. Y. Zhao, F. Li, Z. Sun, Y. Zhang, L. Xu, A novel oxidation state Keggin-type isopolyoxomolybdate $(C_3H_5N_2)_4H[Mo^{VI}_{0.5}Mo^{VI}_{12}O_{40}]$: synthesis, structural characterization and electrocatalytic properties, *Inorg. Chem. Commun.* **70**, 83 (2016)
51. A. Sharma, S.K. Mehta, S. Singh, S. Gupta, Synthesized colloidal-supported Pt and bimetallic Pt–Mo nanoparticles as electrocatalyst in oxidation of methanol in alkaline solution. *J. Appl. Electrochem.* **46**(1), 27–38 (2016)
52. C.V. Krishnan, M. Garnett, B. Hsiao, B. Chu, Electrochemical measurements of isopolyoxomolybdates: 1. pH dependent behavior of sodium molybdate. *Int. J. Electrochem. Sci.* **2**, 29 (2007)
53. J. Jońca, C. Barus, W. Giraud, D. Thouron, V. Garçon, M. Comtat, Electrochemical behaviour of isopoly- and heteropolyoxomolybdates formed during anodic oxidation of molybdenum in seawater. *Int. J. Electrochem. Sci.* **7**(7325) (2012)
54. P. Enghag, *Encyclopaedia of the Elements*, (Wiley-VCH, Weinheim, 2004) p. 590
55. C.H. Hamann, A. Hamnett, W. Vielstich, *Electrochemistry*, (Wiley-VCH, Weinheim, 2007) p 257
56. R. Zhou, Y. Zheng, M. Jaroniec, S.Z. Qiao, Determination of the electron transfer number for the oxygen reduction reaction: from theory to experiment. *ACS Catal.* **6**(7), 4720–4728 (2016)